IX CONGRESSO BRASILEIRO DE
ENGENHARIA E CIÊNCIAS TÉRMICAS
9th BRAZILIAN CONGRESS OF THERMAL
ENGINEERING AND SCIENCES

Paper CIT02-0601

STABILITY OF VISCOPLASTIC FLOW IN ANNULI WITH A ROTATING INNER CYLINDER

Oscar Coronado
oscarcm@mec.puc-rio.br

Paulo Roberto de Souza Mendes
pmendes@mec.puc-rio.br

Marcio da Silveira Carvalho
Departament Mechanical Engineering, Pontifícia Universidade Católica do Rio de Janeiro.
Rua Marquês de São Vicente, 225. Gávea, Rio de Janeiro, 22453-900, Brazil.
msc@mec.puc-rio.br

Abstract. *The superposition of a circular Couette flow and a pressure-driven axial flow in an annulus occurs in many practical applications, such as catalytic chemical reactors, filtration devices, liquid-liquid extractors, journal bearings, and the return flow of drilling mud between the rotating drill string and the stationary wall in oil and gas well drilling. The curved streamlines of the circular Couette flow can cause a centrifugal instability leading to toroidal vortices, well known as Taylor vortices. The presence of these vortices changes the hydrodynamic and heat transfer characteristics of the process. Therefore, it is very important to be able to predict the onset of the instability. Most of the available theoretical and experimental analyses are for Newtonian and viscoelastic (polymeric solutions) liquids. In this work, the effect of the viscoplastic properties of high concentration suspensions on the onset of the Taylor vortices are determined theoretically by solving the conservation equations and searching the critical conditions. The differential equations were solved by the Galerkin / finite element method and the resulting set of non-linear algebraic equations, by Newton's method.*

Keywords: *concentric cylinders, viscoplastic fluid, Taylor instability, finite element method*

1. Introduction

The superposition of a circular Couette flow and a pressure-driven axial flow in an annulus occurs in many practical applications, such as catalytic chemical reactors, filtration devices, liquid-liquid extractors, journal bearings, and the return flow of drilling mud between the rotating drill string and the stationary wall in oil and gas well drilling. The pioneering work of Taylor, 1923, showed that in the case of vanishing axial pressure gradient, the purely azimuthal flow, i.e. a pure Couette flow, can evolve to a flow containing recirculating vortex rings if the angular speed of the inner cylinder is above a critical value. This type of flow instability is known as *Taylor instability.* The same instability also occurs in the case of non-vanishing pressure gradient in the axial direction. At a certain combination of axial flow rate and angular speed of the cylinder, a transition from a spiral Couette-Poiseuille flow to an axial flow with toroidal Taylor vortices takes place. Figure 1 illustrates the different flow patterns that have been observed.

The flow pattern can drastically affect the transport phenomena that occurs in the applications mentioned before. In the case of continuous reactors, the yield is maximized if mixing in the transverse direction is large and in the longitudinal direction is small. Therefore, the process can be optimized by using annular flow through concentric cylinders rotating at angular speed that Taylor vortices are present. In the case of well drilling, the transport of rock chipping, the diffusion of gas, the build-up of mud cake on the formation wall and the required pressure to pump the drilling mud are all affected by the characteristics of the flow between the rotating drill and the stationary bore hole wall.

The stability of Newtonian flow between concentric rotating cylinder has been extensively studied in the past. The main goal was to determine experimentally and theoretically the critical operating condition at the onset of the instability at different flow configurations. The critical conditions are usually reported in terms of a critical Taylor number $Ta \equiv \rho\omega_{in}r_i d/\mu$. The experimental investigations consisted of flow visualization to observe the different flow patterns with and without imposed axial flow. The main contributions are by Gravas, 1978; Andereck, 1986 and Lueptw, 1992. The theoretical analysis leads to an eigenproblem. The first contributions used perturbation analysis and were restricted to narrow gaps and axisymmetric disturbances. The methods were later extended to arbitrarily wide annular gaps. The main contributions are by Chandrasekhar, 1961; Diprima, 1960 and Lee, 2001.

In many practical situations the liquid of interest is non-Newtonian. In the specific case of the flow in the annulus between the rotating drill and the rock formation, the rheological behavior of the mud changes the critical conditions at which Taylor vortices appear. Drilling mud is a high concentrated colloidal suspension with a strong shear-thinning behavior and negligible elasticity, well described by a Generalized Newtonian Model with a Carreau viscosity function. The effect of the rheological parameters of viscoplastic liquids on the critical conditions for the onset of the Taylor instability is still a matter of research (see Escudier, 1995 and Lockett, 1992).

In this work, the critical Taylor number in the case of no imposed axial flow at different geometrical configuration, i.e. inner-to-outer cylinder radius ratio r_i/r_o, and different rheological parameters is determined by tracking the solution path as the Taylor number rises. The critical condition is characterized by the sudden appearance of an axial and radial velocity component. At each condition, the system of differential equation is solved by the Galerkin / finite element method. The resulting set of non-linear algebraic equations is solved by Newton's method.

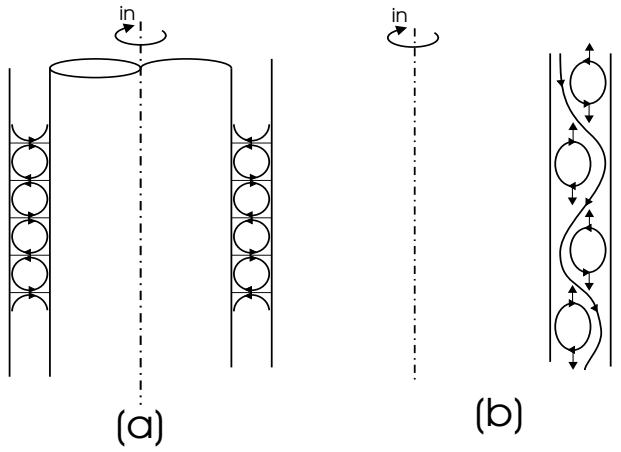

Figure 1: Observed flow patterns: (a)Taylor vortices (b) Helical vortices.

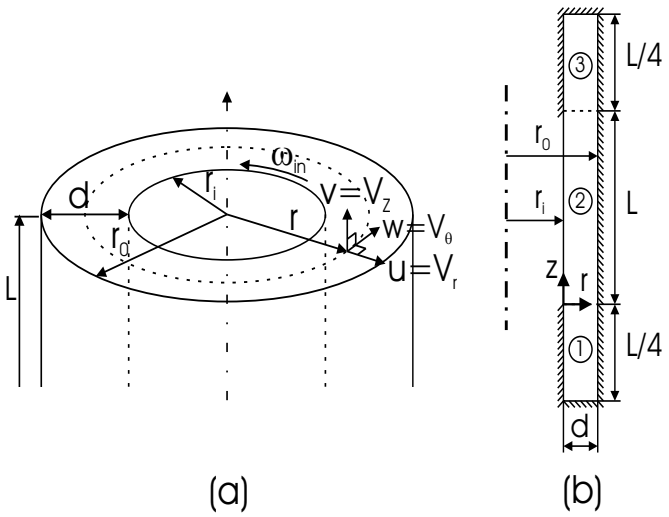

Figure 2: Geometrical configuration of flow between concentric rotating cylinders.

2. Mathematical Model

The configuration of the flow analyzed in this work is shown in Fig. 2. The inner cylinder has a radius equal to r_i and it is rotating at a speed of ω_{in}. The radius of the outer cylinder is equal to r_o and it is stationary. The gap between the cylinders is $d = r_o - r_i$. Most of the work presented in the literature considered the annular space infinitely long, i.e. end effects are neglected. Because in most practical applications end effects are present, here the length L of the annular space was taken to be finite. The end effects are modelled by a region, $L/4$ long, between stationary cylinders at both extremes of the annular space.

The phase diagram of the flow states between infinitely long cylinders, characterized by the average axial component of the velocity field $\| \overline{v_z} \|$, as a function of the angular speed of the inner cylinder ω_{in} is sketched in Fig. 3. The continuous line represents stable states and the dashed line corresponds to unstable flow states. Flow states that have $\| \overline{v_z} \| = 0$ do not exhibit vortices and those characterized by $\| \overline{v_z} \| \neq 0$ have a vortex structure. At the critical Taylor number $Ta = Ta^*$, a pitchfork bifurcation occurs. The flow without vortices becomes unstable and the stable states are those that contain recirculating vortices. Experiments has shown that just beyond the onset of the instability, the vortices formed are steady and axisymmetric.

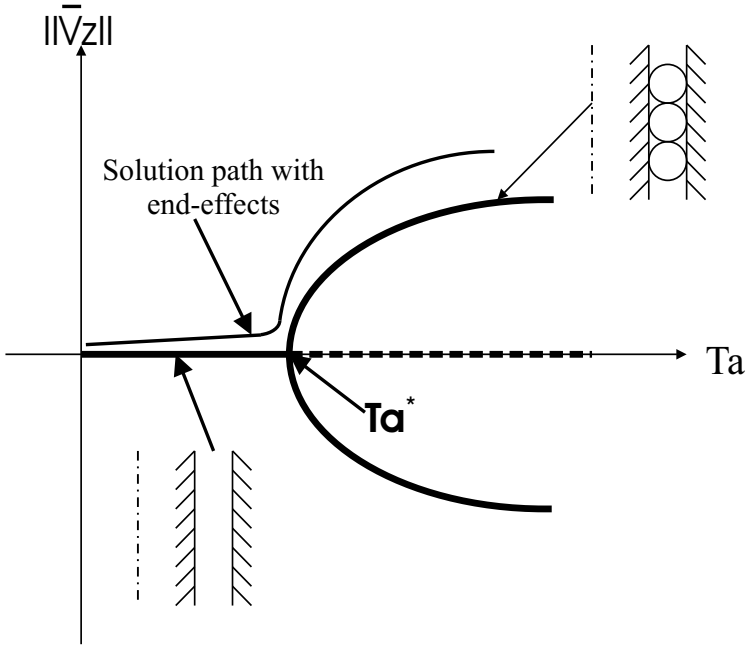

Figure 3: Sketch of the phase diagram of the flow between concentric rotating cylinders. Continuous lines represent stable branches.

The tactic used here to find the critical Taylor number is to construct a solution path as a function of Taylor number by solving the complete three-dimensional Navier-Stokes equations for steady, axisymmetric flow. Because of the end effects, even at very small Taylor number, the axial velocity component will not be exactly equal to zero. The expected solution path is also sketched in Fig.(3). It should lie close to the stable branches of the diagram. Near the critical Taylor number, it should show a sudden change in the average axial velocity component, an indication of the instability. This procedure avoids the solution of the eigenproblem that comes from the stability analysis formulation developed by previous researchers.

2.1. Conservation equations

The liquid motion is governed by the momentum and continuity equations for axisymmetric and steady flows.

$$\rho\left(v\frac{\partial u}{\partial z} - \frac{w^2}{r} + u\frac{\partial u}{\partial r}\right) = \frac{1}{r}\frac{\partial}{\partial r}(r\tau_{rr}) - \frac{\tau_{\theta\theta}}{r} + \frac{\partial \tau_{zr}}{\partial z} \tag{1}$$

$$\rho\left(v\frac{\partial v}{\partial z} + u\frac{\partial v}{\partial r}\right) = \frac{1}{r}\frac{\partial}{\partial r}(r\tau_{rz}) + \frac{\partial \tau_{zz}}{\partial z} \tag{2}$$

$$\rho\left(v\frac{\partial w}{\partial z} + \frac{uw}{r} + u\frac{\partial w}{\partial r}\right) = \frac{\partial \tau_{r\theta}}{\partial r} + \frac{2}{r}\tau_{r\theta} + \frac{\partial \tau_{z\theta}}{\partial z} \tag{3}$$

$$\frac{1}{r}\frac{\partial}{\partial r}(ru) + \frac{\partial v}{\partial z} \tag{4}$$

The boundary conditions are:

$$r = r_i; 0 < z < L: \quad u = 0, v = 0 \quad \text{and} \quad w = \omega_{in} r_i \tag{5}$$

$$r = r_i; -L/4 < z < 0 \text{ or } L < z < L + L/4: \quad u = v = w = 0 \tag{6}$$

$$r = r_o: \quad u = v = w = 0 \tag{7}$$

$$z = -L/4 \text{ or } z = L + L/4: \quad u = v = w = 0 \tag{8}$$

The relevant dimensionless parameters for this situation are:

1. Radius ratio, $\Pi \equiv r_i/r_o$
2. Aspect ratio, $\Gamma \equiv L/d$
3. Taylor number, $Ta \equiv \rho\omega_{in} r_i d/\mu$

2.2. Non Newtonian model

Drilling mud is a high concentrated colloidal suspension and it is well described by a Generalized Newtonian Model. The stress tensor $\underline{\tau}$ is a non-linear function of the rate of deformation tensor $\underline{\underline{2D}}$:

$$\underline{\tau} = \eta(\dot{\gamma})\underline{\underline{2D}} \tag{9}$$

The viscosity dependence on shear rate can be represented by a Carreau model:

$$\frac{\eta - \eta_\infty}{\eta_0 - \eta_\infty} = [1 + (\lambda\dot{\gamma})^a]^{\frac{n-1}{a}} \tag{10}$$

η_0 is the viscosity at low shear rate, η_∞ is the viscosity at high shear rate, λ is a time constant, n is the power-law index, and $\dot{\gamma}$ is the shear rate. It is given by

$$\dot{\gamma} = \sqrt{2tr\underline{\underline{D}}^2} = \sqrt{2\left[\left(\frac{\partial v}{\partial z}\right)^2 + \left(\frac{u}{r}\right)^2 + \left(\frac{\partial u}{\partial r}\right)^2\right] + \frac{1}{2}\left[\left(\frac{\partial w}{\partial z}\right)^2 + \left(\frac{\partial u}{\partial z} + \frac{\partial v}{\partial r}\right)^2 + \left(\frac{\partial w}{\partial r} - \frac{w}{r}\right)^2\right]} \tag{11}$$

2.3. Solution of the differential equations

The set of differential equations coupled with the constitutive model was solved by the Galerkin / finite element method. The velocity and pressure field were represented in terms of basis functions:

$$u = \sum_{j=1}^{n} U_j\phi_j\,;\; v = \sum_{j=1}^{n} V_j\phi_j\,;\; w = \sum_{j=1}^{n} W_j\phi_j \;\text{ and }\; p = \sum_{j=1}^{m} P_j\chi_j \tag{12}$$

Biquadratic basis functions ϕ_i were used to represent the velocity and piece-wise linear discontinuous functions χ_i were used to represent the pressure field. The corresponding weighted residuals of the Galerkin's method are:

$$R^i_{mr} = \int_{\overline{\Omega}} \left\{\rho\left(v\frac{\partial u}{\partial z} - \frac{w^2}{r} + u\frac{\partial u}{\partial r}\right)\phi_i + \frac{\partial\phi_i}{\partial z}\tau_{rz} + \frac{\phi_i}{r}\tau_{\theta\theta} + \frac{\partial\phi_i}{\partial r}\tau_{rr} - \rho g\phi_i\right\} r|\underline{J}|d\overline{\Omega} + BI; \quad i = 1,\ldots n \tag{13}$$

$$R^i_{m\theta} = \int_{\overline{\Omega}} \left\{\rho\left(v\frac{\partial w}{\partial z} + \frac{wu}{r} + u\frac{\partial w}{\partial r}\right)\phi_i + \frac{\partial\phi_i}{\partial z}\tau_{\theta z} - \frac{\phi_i}{r}\tau_{r\theta} + \frac{\partial\phi_i}{\partial r}\tau_{\theta r}\right\} r|\underline{J}|d\overline{\Omega} + BI; \quad i = 1,\ldots n \tag{14}$$

$$R^i_{mz} = \int_{\overline{\Omega}} \left\{\rho\left(v\frac{\partial v}{\partial z} + u\frac{\partial v}{\partial r}\right)\phi_i + \frac{\partial\phi_i}{\partial z}\tau_{zz} + \frac{\phi_i}{r}\tau_{zr}\right\} r|\underline{J}|d\overline{\Omega} + BI; \quad i = 1,\ldots n \tag{15}$$

$$R^i_c = \int_{\overline{\Omega}} \left(\frac{u}{r} + \frac{\partial u}{\partial r} + \frac{\partial v}{\partial z}\right)\chi_i r|\underline{J}|d\overline{\Omega}; \quad i = 1,\ldots m \tag{16}$$

Once all the variables are represented in terms of the basis functions, the system of partial differential equations reduces to simultaneous algebraic equations for the coefficients of the basis functions of all the fields. This set of equations is non-linear and sparse. It was solved by Newton's method:

$$\underline{u}_{(k+1)} = \underline{u}_{(k)} + \underline{\Delta u} \tag{17}$$

$$\underline{\underline{J}}\,\underline{\Delta u} = -\underline{R} \tag{18}$$

$\mathbf{u}$ is the vector of the unknowns coefficients of the basis functions for the velocity and pressure, $\underline{R}$ is the vector of the weighted residuals, and $\underline{\underline{J}}$ is the Jacobian matrix of sensitivities of the residuals to the unknowns:

$$J_{ij} = \begin{bmatrix} \frac{\partial R_{mz}}{\partial V_j} & \frac{\partial R_{mz}}{\partial W_j} & \frac{\partial R_{mz}}{\partial U_j} & \frac{\partial R_{mz}}{\partial P_j} \\ \frac{\partial R_{m\theta}}{\partial V_j} & \frac{\partial R_{m\theta}}{\partial W_j} & \frac{\partial R_{m\theta}}{\partial U_j} & \frac{\partial R_{m\theta}}{\partial P_j} \\ \frac{\partial R_{mr}}{\partial V_j} & \frac{\partial R_{mr}}{\partial W_j} & \frac{\partial R_{mr}}{\partial U_j} & \frac{\partial R_{mr}}{\partial P_j} \\ \frac{\partial R_c}{\partial V_j} & \frac{\partial R_c}{\partial W_j} & \frac{\partial R_c}{\partial U_j} & \frac{\partial R_c}{\partial P_j} \end{bmatrix} \tag{19}$$

The entries of the Jacobian matrix are given by:

$$\frac{\partial R^i_{mr}}{\partial U_j} = \int_{\overline{\Omega}} \left\{ \rho\phi_i \left(v\frac{\partial \phi_j}{\partial z} + \phi_j \frac{\partial u}{\partial r} + u\frac{\partial \phi_j}{\partial r} \right) + \frac{\partial \phi_i}{\partial z}\frac{\partial \tau_{rz}}{\partial U_j} + \frac{\phi_i}{r}\frac{\partial \tau_{\theta\theta}}{\partial U_j} + \frac{\partial \phi_i}{\partial r}\frac{\partial \tau_{rr}}{\partial U_j} \right\} r|\underline{J}|d\overline{\Omega} \tag{20}$$

$$\frac{\partial R^i_{mr}}{\partial V_j} = \int_{\overline{\Omega}} \left\{ \rho\phi_i \left(\phi_j \frac{\partial u}{\partial z} \right) + \frac{\partial \phi_i}{\partial z}\frac{\partial \tau_{rz}}{\partial V_j} + \frac{\phi_i}{r}\frac{\partial \tau_{\theta\theta}}{\partial V_j} + \frac{\partial \phi_i}{\partial r}\frac{\partial \tau_{rr}}{\partial V_j} \right\} r|\underline{J}|d\overline{\Omega} \tag{21}$$

$$\frac{\partial R^i_{mr}}{\partial W_j} = \int_{\overline{\Omega}} \left\{ \rho\phi_i \left(-\phi_j \frac{2w}{r} \right) + \frac{\partial \phi_i}{\partial z}\frac{\partial \tau_{rz}}{\partial W_j} + \frac{\phi_i}{r}\frac{\partial \tau_{\theta\theta}}{\partial W_j} + \frac{\partial \phi_i}{\partial r}\frac{\partial \tau_{rr}}{\partial W_j} \right\} r|\underline{J}|d\overline{\Omega} \tag{22}$$

$$\frac{\partial R^i_{mr}}{\partial P_j} = \int_{\overline{\Omega}} \left\{ \frac{\partial \phi_i}{\partial z}\frac{\partial \tau_{rz}}{\partial P_j} + \frac{\phi_i}{r}\frac{\partial \tau_{\theta\theta}}{\partial P_j} + \frac{\partial \phi_i}{\partial r}\frac{\partial \tau_{rr}}{\partial P_j} \right\} r|\underline{J}|d\overline{\Omega} \tag{23}$$

$$\frac{\partial R^i_{m\theta}}{\partial U_j} = \int_{\overline{\Omega}} \left\{ \rho\phi_i \left(\frac{w}{r}\phi_j + \phi_j \frac{\partial w}{\partial r} \right) + \frac{\partial \phi_i}{\partial z}\frac{\partial \tau_{\theta z}}{\partial U_j} - \frac{\phi_i}{r}\frac{\partial \tau_{r\theta}}{\partial U_j} + \frac{\partial \phi_i}{\partial r}\frac{\partial \tau_{\theta r}}{\partial U_j} \right\} r|\underline{J}|d\overline{\Omega} \tag{24}$$

$$\frac{\partial R^i_{m\theta}}{\partial V_j} = \int_{\overline{\Omega}} \left\{ \rho\phi_i \left(\phi_j \frac{\partial w}{\partial z} \right) + \frac{\partial \phi_i}{\partial z}\frac{\partial \tau_{\theta z}}{\partial V_j} - \frac{\phi_i}{r}\frac{\partial \tau_{r\theta}}{\partial V_j} + \frac{\partial \phi_i}{\partial r}\frac{\partial \tau_{\theta r}}{\partial V_j} \right\} r|\underline{J}|d\overline{\Omega} \tag{25}$$

$$\frac{\partial R^i_{m\theta}}{\partial W_j} = \int_{\overline{\Omega}} \left\{ \rho\phi_i \left(v\frac{\partial \phi_j}{\partial z} + \phi_j \frac{u}{r} + u\frac{\partial \phi_j}{\partial r} \right) + \frac{\partial \phi_i}{\partial z}\frac{\partial \tau_{\theta z}}{\partial W_j} - \frac{\phi_i}{r}\frac{\partial \tau_{r\theta}}{\partial W_j} + \frac{\partial \phi_i}{\partial r}\frac{\partial \tau_{\theta r}}{\partial W_j} \right\} r|\underline{J}|d\overline{\Omega} \tag{26}$$

$$\frac{\partial R^i_{m\theta}}{\partial P_j} = \int_{\overline{\Omega}} \left\{ \frac{\partial \phi_i}{\partial z}\frac{\partial \tau_{\theta z}}{\partial P_j} - \frac{\phi_i}{r}\frac{\partial \tau_{r\theta}}{\partial P_j} + \frac{\partial \phi_i}{\partial r}\frac{\partial \tau_{\theta r}}{\partial P_j} \right\} r|\underline{J}|d\overline{\Omega} \tag{27}$$

$$\frac{\partial R^i_{mz}}{\partial U_j} = \int_{\overline{\Omega}} \left\{ \rho\phi_i \left(\phi_j \frac{\partial v}{\partial r} \right) + \frac{\partial \phi_i}{\partial z}\frac{\partial \tau_{zz}}{\partial U_j} - \frac{\partial \phi_i}{\partial r}\frac{\partial \tau_{zr}}{\partial U_j} \right\} r|\underline{J}|d\overline{\Omega} \tag{28}$$

$$\frac{\partial R^i_{mz}}{\partial V_j} = \int_{\overline{\Omega}} \left\{ \rho\phi_i \left(\phi_j \frac{\partial v}{\partial z} + v\frac{\partial \phi_j}{\partial z} + u\frac{\partial \phi_j}{\partial r} \right) + \frac{\partial \phi_i}{\partial z}\frac{\partial \tau_{zz}}{\partial V_j} + \frac{\partial \phi_i}{\partial r}\frac{\partial \tau_{zr}}{\partial V_j} \right\} r|\underline{J}|d\overline{\Omega} \tag{29}$$

$$\frac{\partial R^i_{mz}}{\partial W_j} = \int_{\overline{\Omega}} \left\{ \frac{\partial \phi_i}{\partial z}\frac{\partial \tau_{zz}}{\partial W_j} + \frac{\partial \phi_i}{\partial r}\frac{\partial \tau_{zr}}{\partial W_j} \right\} r|\underline{J}|d\overline{\Omega} \tag{30}$$

$$\frac{\partial R^i_{mz}}{\partial P_j} = \int_{\overline{\Omega}} \left\{ \frac{\partial \phi_i}{\partial z}\frac{\partial \tau_{zz}}{\partial P_j} + \frac{\partial \phi_i}{\partial r}\frac{\partial \tau_{zr}}{\partial P_j} \right\} r|\underline{J}|d\overline{\Omega} \tag{31}$$

$$\frac{\partial R^i_c}{\partial U_j} = \int_{\overline{\Omega}} \left\{ \frac{\phi_j}{r} + \frac{\partial \phi_j}{\partial r} \right\} \chi_i r|\underline{J}|d\overline{\Omega} \tag{32}$$

$$\frac{\partial R^i_c}{\partial V_j} = \int_{\overline{\Omega}} \left\{ \frac{\partial \phi_j}{\partial z} \right\} \chi_i r|\underline{J}|d\overline{\Omega} \tag{33}$$

$$\frac{\partial R^i_c}{\partial W_j} = 0 \tag{34}$$

$$\frac{\partial R^i_c}{\partial P_j} = 0 \tag{35}$$

The linear system of equations at each Newton iteration was solved using a frontal solver.

3. Results

The aspect ratio of the annular space was held constant at $\Gamma = 10$ in all calculations presented here. The critical Taylor number was determined as a function of the radii ratio and rheological properties of the liquid.

3.1. Newtonian Liquids

The solution path obtained at radii ratio $\Pi = 0.6$ and rising Taylor number (angular velocity of the inner cylinder) is shown in Fig. 4. Each flow state is characterized by the ratio of the average axial to the tangential velocity $\overline{V_z}/\overline{V_\theta}$. At small Taylor number, the average axial velocity is less than 1% of the azimuthal velocity. The weak axial flow is caused by the end effects. At Taylor number close to 70, there is a sudden change on the growth rate of the average axial velocity. This behavior indicates the onset of the instability. The critical Taylor number is estimated by the intersection of the tangents of the two regions of the path, as indicated in Fig. 4. The critical Taylor number for this situation was $Ta^* = 67.7$. Figure 5 shows evolution of the projection of the streamlines on the $r - z$ plane, i.e. the vortex pattern, as Taylor number rises. $z = L$ represents the position of the end of the rotating portion of the inner cylinder. At $Ta = 33.4$, the flow is mainly in the azimuthal direction and far from the edges, there is no evident recirculation pattern. It is important to observe that, even at low Taylor number, there is a small recirculation at both extremes of the flow domain due to the velocity discontinuity of the boundary condition at the inner cylinder. At Taylor number larger than the critical value, e.g. $Ta = 80$, the presence of Taylor vortices is evident. The calculated aspect ratio of each recirculation cell $h/d = 0.99$ agrees well with experimental measurements.

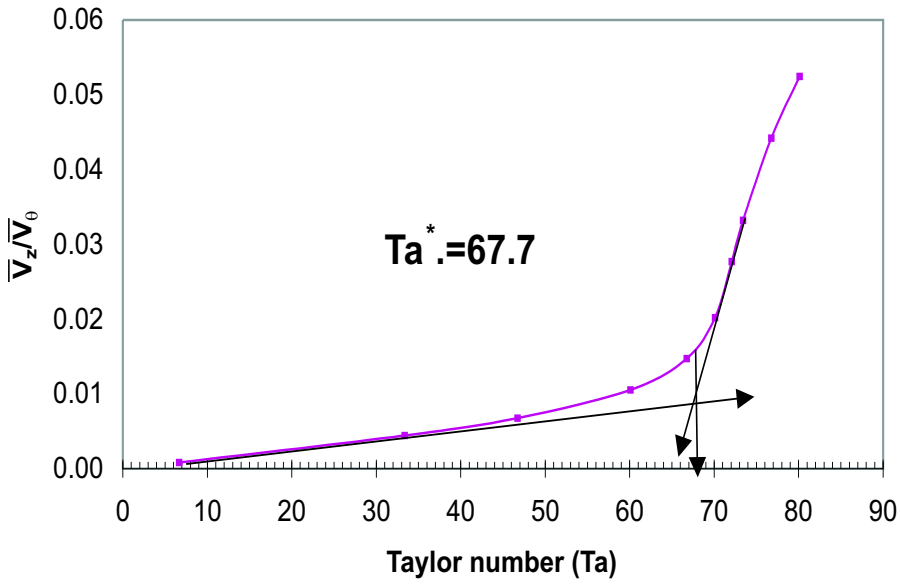

Figure 4: Solution path for Newtonian liquid as Taylor number rises. Radii ratio is $\Pi = 0.6$.

A solution path similar to the one presented in Fig. 4 was constructed at different radii ratio Π and a critical Taylor number was estimated at each condition. The results are summarized in Fig. 6. The critical Taylor number rises as the gap between the two cylinders becomes narrower. The azimuthal flow in narrow gaps is more stable than the flow in wide gaps between the two cylinders. The plot also shows the critical Taylor number obtained experimentally by different researchers and presented by Lueptw, 1992. The agreement between the predictions reported here the experiments is excellent.

The onset of Taylor vortices affects the azimuthal velocity profile and consequently the shear stress at the cylinder walls. The velocity profile before and after the onset of the instability is shown in Fig. 7. At Taylor number higher than the critical value, the profile is shown at two different $z = constant$ planes, e.g. one that corresponds to the plane that divides two adjacent vortex cells and the other that passes through the vortex center. The azimuthal shear stress rises after the onset of the instability, which may have an impact on the power necessary to rotate the inner cylinder.

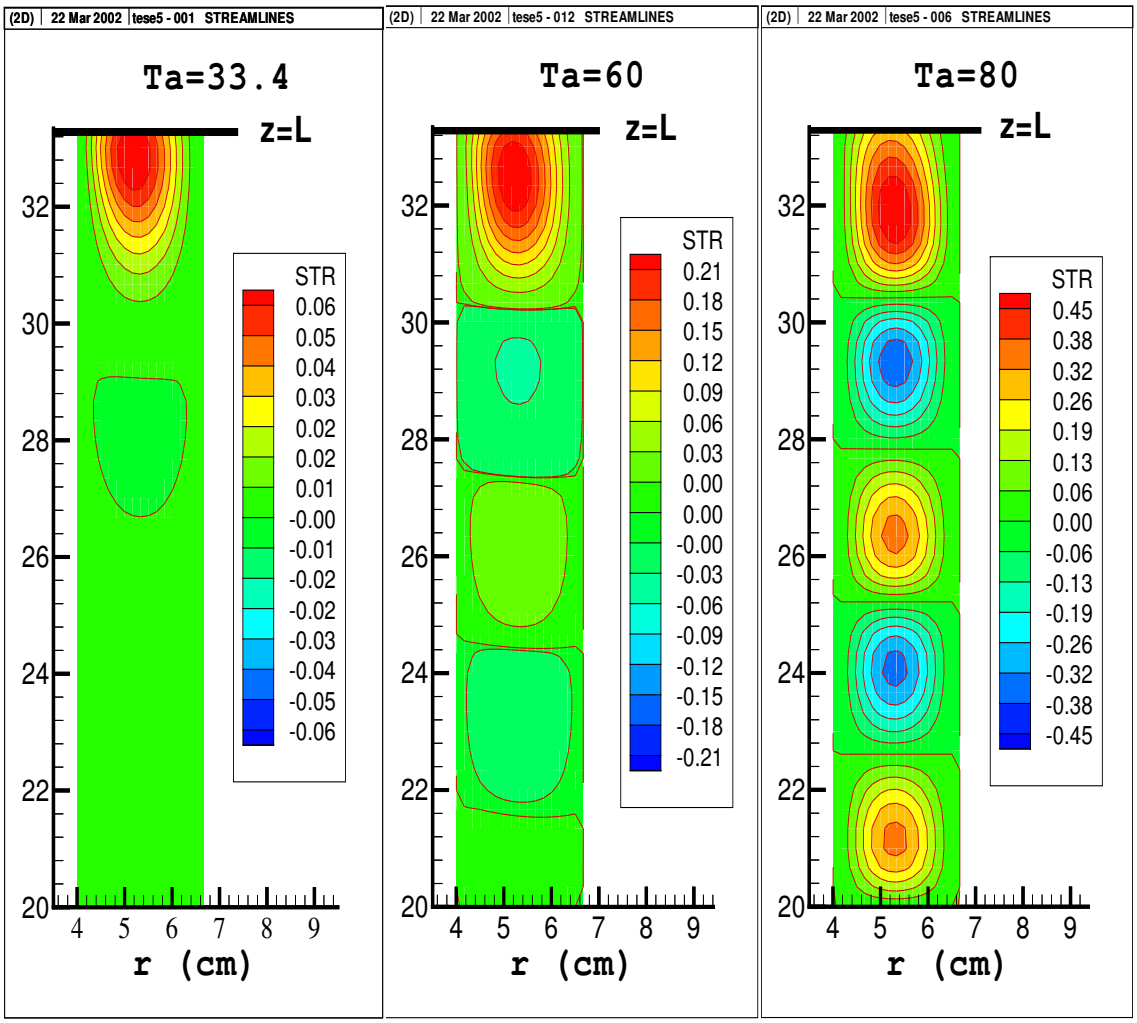

Figure 5: Evolution of the vortex pattern as Taylor number rises.

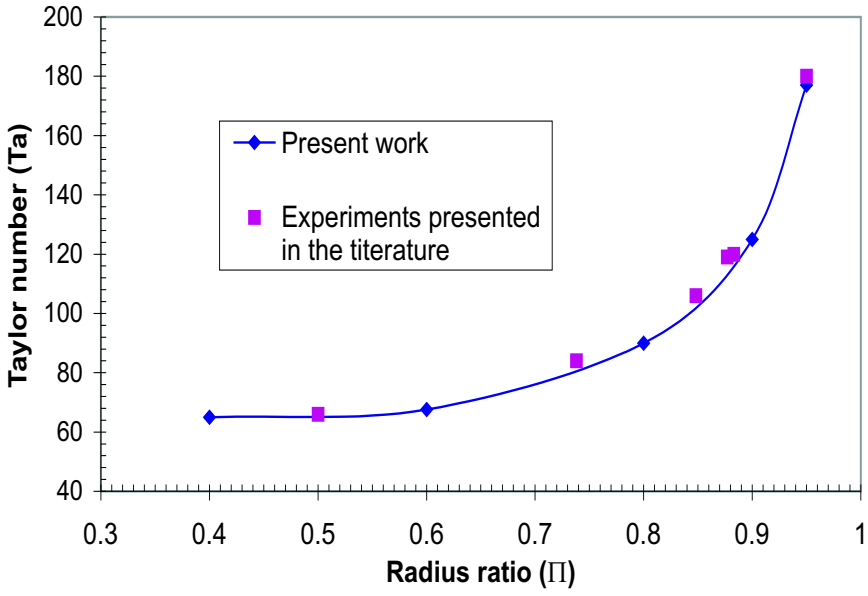

Figure 6: Critical Taylor number for Newtonian liquids as a function of radii ratio $\Pi \equiv r_i/r_o$

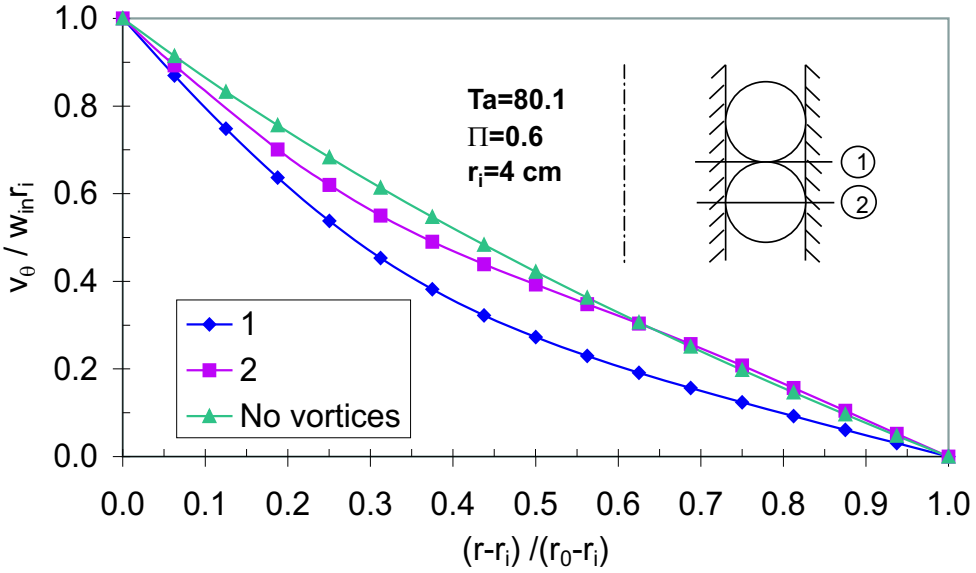

Figure 7: Azimuthal velocity profile before and after the appearance of Taylor vortices.

3.2. Viscoplastic Liquids

The effect of the viscoplastic liquid rheology on the onset of Taylor instability was analyzed here by varying the high shear viscosity η_∞ and the power-law index n of the Carreau viscosity function. The time constant and the low shear viscosity were held constant and equal to $\lambda = 0.1\text{s}^{-1}$ and $\eta_0 = 0.004$Pa.s. Solution paths similar to the one presented in Fig. 4 were constructed at different values of the rheological parameters. The predicted critical Taylor number at a radii ratio of $\Pi = 0.95$ is shown in Fig. 8.Taylor number is defined in terms of the low shear viscosity, e.g. $Ta = \rho\omega_{in} r_i d/\eta_0$. The predicted critical Taylor number for Newtonian liquid was $Ta^* = 178$. As the power-law index n and the high-shear viscosity η_∞ falls, the onset of the Taylor instability occurs at lower inner cylinder speed. In some cases, the critical speed can be half of the speed at which the instability occurs with Newtonian liquids. One possible explanation for the early onset of the instability in the case of viscoplastic liquids is that the local viscosity in regions of high shear rate can by much smaller than η_0 due to the shear-thinning behavior of the liquid.

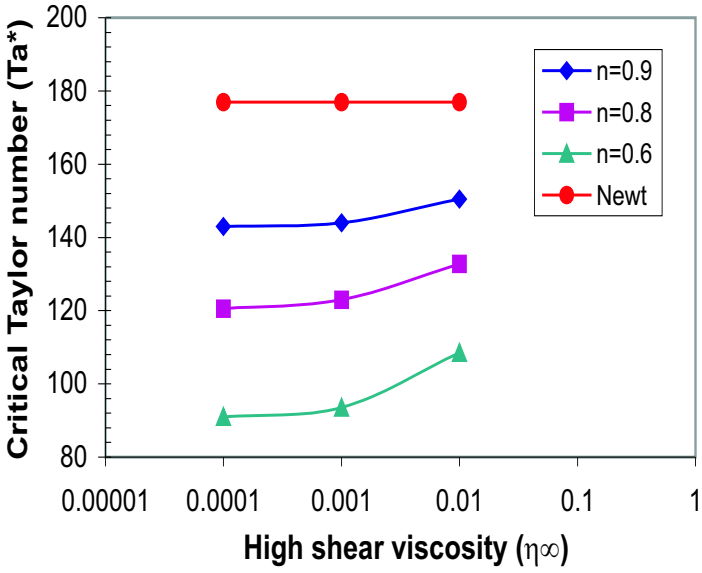

Figure 8: Critical Taylor number as a function of the viscoplastic rheological parameters. Radii ratio is $\Pi = 0.95$

The effect of radii ratio Π on the onset of the instability when viscoplastic liquids are used is presented in Fig. 9. For wide gaps, i.e. $\Pi < 0.8$, the shear thinning behavior of the liquid does not affect the critical Taylor number for the value of λ explored here. The shear rates that occur in these cases are low enough that the viscosity everywhere in the flow is approximately equal to the low-shear viscosity η_0. At a fixed radii ratio, the critical Taylor number falls as the power-law index decreases. At low power-law index, e.g. $n = 0.6$, the effect of the radii ratio on the critical Taylor number is not monotonic. At radii ratio larger than $\Pi > 0.9$, the critical angular speed falls with rising radii ratio.

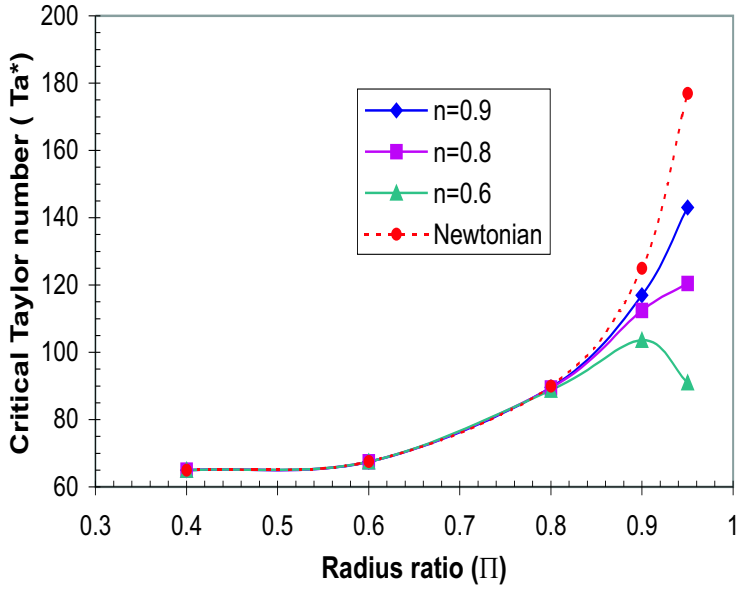

Figure 9: Effect of radii ratio Π on the onset of the instability for viscoplastic liquids.

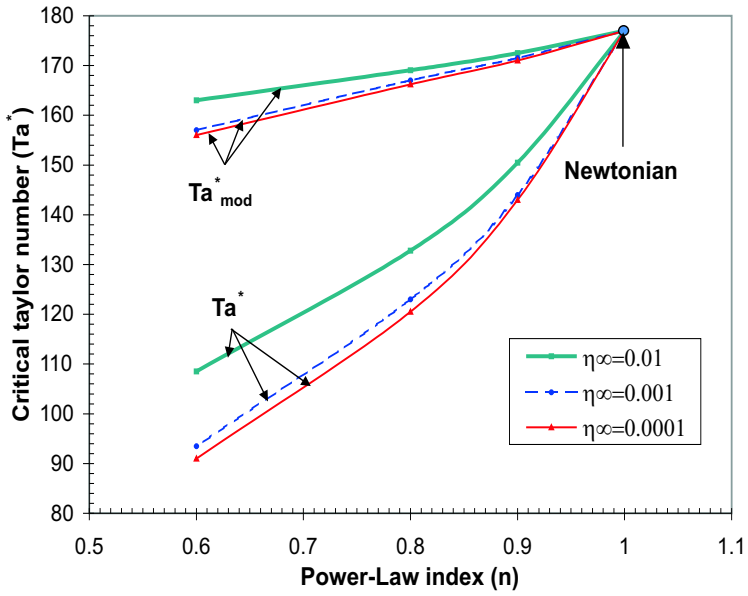

Figure 10: Critical conditions at the onset of the instability presented in terms of the modified Taylor number. Radii ratio is $\Pi = 0.95$.

The critical Taylor number as a function of the power-law index n at three values of the high shear viscosity η_∞ is presented in Fig. 10. The radii ratio is fixed at $\Pi \equiv r_i/r_o = 0.95$. For Newtonian liquid, the onset of the instability occurs at $Ta^* = 178$. As mentioned before, the relative decrease in the critical speed in the case of shear thinning liquids can be as high as 50%. Because the viscosity is a strong function of the shear rate, in this situation it is more appropriate to define a Taylor number based on a characteristic viscosity $\eta_c = \eta(\dot{\gamma}_c)$, called here the modified Taylor number Ta_{mod}, and defined as

$$Ta_{mod} \equiv \frac{\rho \omega_{in} r_i d}{\eta(\dot{\gamma}_c)} \tag{36}$$

The characteristic shear rate is $\dot{\gamma}_c = \omega_{in} r_i / d$. Figure 10 also presents the critical conditions in terms of the critical modified Taylor number Ta^*_{mod}. If the pseudoplastic behavior of the liquid is taken into account on the definition of the Taylor number of the flow, the variation of the critical value at the onset of Taylor instability becomes much less sensitive to the rheological parameters. For the cases analyzed in this work, the maximum relative variation was approximately 12%. Therefore, for an estimation of the critical angular speed at which the azimuthal flow of viscoplastic liquids between rotating cylinders becomes unstable, a modified Taylor number, defined in terms of a characteristic viscosity, can be used. The instability occurs at approximately $Ta^*_{mod} = Ta^*$ for Newtonian liquids.

4. Final Comments

The onset of Taylor vortices that completely changes the flow pattern between rotating concentric cylinders can affect the transport phenomena that occurs in many practical applications. Taylor instability of Newtonian liquids has been extensively studied by theory and experiments. However, in many applications, the flowing liquid is a suspension with viscoplastic behavior. The effect of the rheological parameters on the critical conditions at the onset of Taylor instability is still not completely understood.

In this work, the critical operating condition at different geometrical configurations and rheological parameters is determined by tracking the solution path as Taylor number rises and searching for sudden changes on the axial and radial velocity components. The system of differential equations is solved by the Galerkin / finite element method and the resulting set of non-linear equation is solved by Newton's method. The results show that when the liquid is shear-thinning the appearance of Taylor vortices occurs at lower angular speed.

5. Acknowledgments

Oscar Coronado was supported with a scholarship from CAPES. This work was funded by grants from CNPq and FAPERJ.

6. References

Andereck, C.D.; Liu, S. S. H., 1986, Flow Regimes in a Circular Couette System with Independently Rotating Cylinders, "Journal of Fluid Mechanics", Vol. 164, pp. 15–183.

Chandrasekhar, S., 1961, "Hydrodynamic and Hydromagnetic Stability", Dover Publications, INC.

Diprima, R., 1960, The Stability of a Viscous Fluid between Rotating Cylinders with an Axial Flow, "Journal of Fluid Mechanics", Vol. 9, pp. 621–631.

Escudier, M.P.; Gouldson, I., 1995, Concentric Annular Flow with Centerbody Rotation of a Newtonian and Shear-Thinning Liquid, "Intenational Journal of Heat and Fluid Flow", Vol. 16, pp. 156–162.

Gravas, N., M. B., 1978, Instability of Viscous Axial Flow in Annuli Having a Rotating Inner Cylinder, "Journal of Fluid Mechnics", Vol. 6(2), pp. 385–394.

Lee, M., 2001, The Stability of Spiral Flow between Coaxial Cylinders, "Computers and Mathematics with Applications", Vol. 41, pp. 289–300.

Lockett, T.J.; Richardson, S. W. W., 1992, The Stability of Inelastic non-Newtonian Fluids in Couette between Concentri Cylinders: a Finite-Element Study, "Journal of non-Newtonian Fluid Mechanics", Vol. 43, pp. 165–177.

Lueptw, R.M.; Docter, A. M. K., 1992, Stability of Axial Flow in an Annulus with a Rotating Inner Cylinder, "Physics of Fluids A - Fluid Dynamics", Vol. 11, pp. 2446–2455.

Taylor, G., 1923, Stability of a Viscous Liquid Contained between two Rotating Cylinders, "Phil. Trans. R. Soc. London", Vol. VIII, pp. 289–345.